Thermal Performance Expectations of the Advanced Stirling Convertor Over a Range of Operating Scenarios

Terry V. Reid[1] and Rodger W. Dyson[2]
NASA Glenn Research Center, Cleveland, Ohio, 44135

The Advanced Stirling Radioisotope Generator (ASRG) will enable various missions such as small body sample return, atmospheric missions around Venus, as well as long-duration deep space missions. Analysis of the temperature distributions are performed on an Advanced Stirling Convertor, and the results are compared with available experimental measurements. This analysis includes applied environmental conditions that are similar to those that will be experienced while the convertor is in operation. The applied conditions represent a potential mission profile including pre-takeoff sterilization, launch, transit, and return.

The results focus on the anticipated peak temperatures of the magnets in the linear alternator. These results confirm that the ASC can support future missions to deep space targets, extreme environment landers, as well as more conventional goals.

Nomenclature

k_{eff}	=	effective thermal conductivity, W/(m-K)
k_{fluid}	=	fluid thermal conductivity, W/(m-K)
k_{solid}	=	solid thermal conductivity, W/(m-K)
K	=	permeability of the medium, m^2
Q_{IN}	=	heat input
T	=	temperature of helium gas (K)
T_{coil}	=	peak temperature of linear alternator coil, K
T_{magnet}	=	peak temperature of linear alternator magnet, K
T_{PV}	=	peak temperature of linear alternator housing (pressure vessel wall), K
W_e	=	electrical power, W
W_{mech}	=	mechanical power, W
W_{LOSS}	=	linear alternator power loss, W
μ	=	molecular viscosity, kg/(m * s)
ν	=	kinematic viscosity, m^2/s
ρ	=	density, kg/m^3
v_i	=	velocity (*for i = x, y, or z* directions), m/s
η_{LA}	=	linear alternator mechanical-to-electrical conversion efficiency, %
γ	=	porosity of the medium

I. Introduction

Stirling power conversion technology has progressed significantly since it was first patented in the early 1800s. It has developed to the point where it may become a valuable contributing component in a variety of space missions. As NASA Glenn Research Center (GRC) works with Sunpower, Inc., to continue technological advances of what is called the Advanced Stirling Convertor (ASC), its capabilities are continuing to be improved upon.[1–3] In an effort to evaluate the capability of the ASC, NASA is performing tests to provide life, reliability, and performance data. The various models of the ASC can be categorized by the applied nominal hot and cold temperatures and the generated electricity.

[1]Research Engineer, Thermal Energy Conversion Branch, 21000 Brookpark Road/MS 301–2, AIAA Member.
[2]Research Engineer, Thermal Energy Conversion Branch, 21000 Brookpark Road/MS 301–2, AIAA Member.

Recent versions of the ASC include the ASC–E, which has hot-end and cold-end temperatures of 650/60 °C, respectively, and generates 75 W_e. The ASC–0 has hot-end and cold-end temperatures of 650/90 °C, respectively, and generates 70 W_e. The ASC-1a, 1b, and 1HS have hot-end and cold-end temperatures of 850/90 °C, respectively, while generating ~80 W_e nominally. These various hardware models also differ by heater head material and how it is attached to the rest of the convertor (in addition to many other details). The most recent version is the ASC–E2 convertor, which is a forerunner of the convertors that will be integrated into a system by the Department of Energy (DOE) and their system integration contractor Lockheed Martin (LM) to potentially support the Discovery 12 mission as early as 2015.

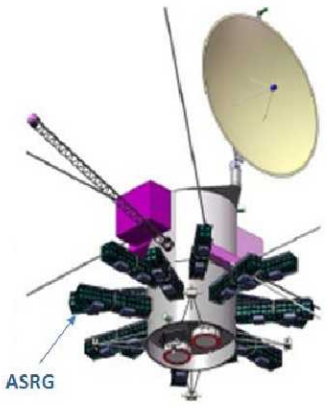

Figure 1. Neptune Flagship Orbiter (Kuiper Belt Object Orbiter).

Other missions are being evaluated where the Advanced Stirling Radioisotope Generator (ASRG) is being considered as a source of the onboard power for a Neptune Flagship Orbiter.[4] The Kuiper Belt Object Orbiter (Fig. 1) is equipped with 28 ASRG modules. Inside of each nominal 140-W_e ASRG module are two ASCs. A single ASRG module is shown in Fig. 2. As the ASC undergoes further development, experimental and computational investigations continue to be performed to assess its durability and reliability. Many of these convertors are hermetically sealed, making it difficult to monitor some internal temperatures of the operating device. High internal temperatures of certain components can have a critical impact on the operating characteristics. It is important to perform a high-fidelity computational analysis in an effort to understand the level of the internal temperature distributions during different operational conditions. A solid CAD model geometry of the ASC–E2 assembly was used to construct an axisymmetric, and a three-dimensional computational model so that temperature distributions throughout the convertor could be calculated.

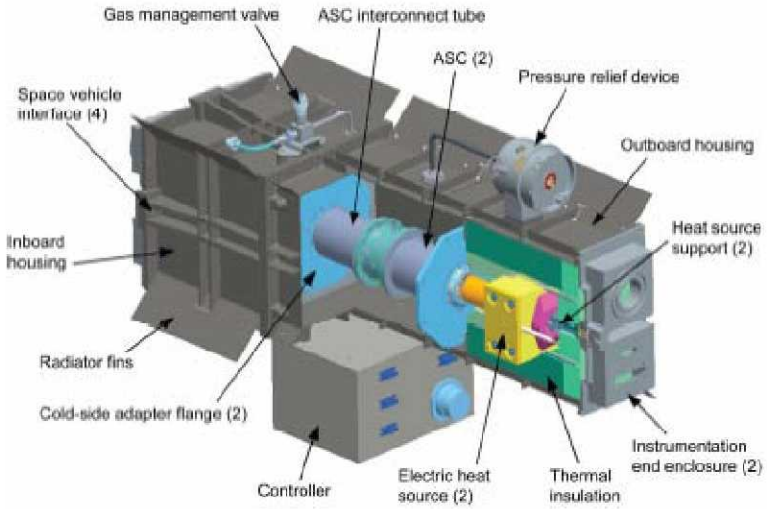

Figure 2. ASRG design by Lockheed Martin.

a) ASRG EU in enclosure on test stand b) ASRG EU and ASC–E #1 and #4 test facility

Figure 3. Facility being prepared for ASRG EU and spare ASC–E convertors. *This facility will house the ASRG EU and the spare pair of ASC–Es.*

II. Convertor Geometry

NASA GRC is working with Sunpower, Inc., to support DOE and LM as they develop the ASRG. The hardware model under test at GRC is the ASRG Engineering Unit (EU) which includes two ASC–E convertors. Testing at the NASA GRC Thermal Energy Conversion Branch is conducted in the Stirling Research Laboratory, as shown in Fig. 3.

The ASC–E2, shown in Fig. 4, utilizes a displacer and a piston, which expands and compresses two separate volumes of gas. When a heat source is applied to the expansion space (at the hot end), the working gas (helium) is shuttled by the displacer between the expansion space and the compression space (at the cold end). The expansion and compression spaces are connected by a porous regenerator, which alternately stores and releases heat as the gas cycles between the two spaces. The thermal energy from the heated helium is temporarily

a) Initial ASC–E2 configuration b) ASC–E2 inside insulation can

Figure 4. Advanced Stirling Convertor ASC–E2.

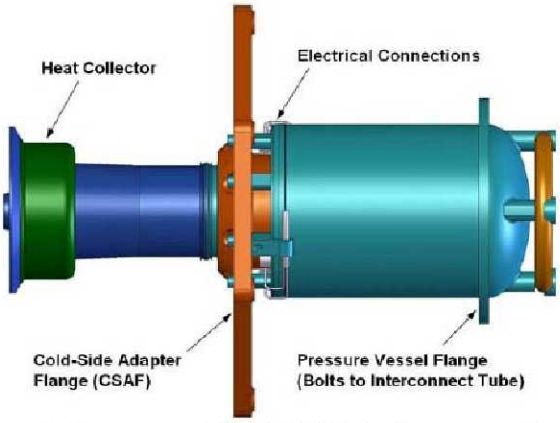

Figure 5. Geometry of the ASC–E2 by Sunpower, Inc.

stored in the porous regenerator as the helium passes from the hot end to the cold end. The cold side adapter flange (CSAF) is used to remove waste heat from the cycle. The reutilization of the stored heat in the regenerator contributes to the enhanced efficiency that is characteristic of a Stirling cycle.

The solid model of the ASC–E2 is shown in Fig. 5. Specifically, heat is applied to the heat collector with the intent of obtaining a target hot-end temperature of 850 °C. In addition, heat is removed from the cycle by the CSAF in a manner so that a target cold-end temperature of 90 °C is obtained at a location where the cold flange meets the rest of the convertor. The power produced in the compression space drives a piston, which is attached to a linear alternator. The linear alternator converts the mechanical power to electrical power, which is then removed from the device and processed for the end user. Because the conversion of mechanical to electrical power is not 100%, the remainder (nonconverted mechanical power) is accounted for as a heat generation source inside the convertor. This will be discussed in detail later in the paper.

III. Modeling Approach

The computational models were constructed using commercial software. The commercial Computational Fluid Dynamics (CFD) grid generator GAMBIT was used to create a meshed model from the solid model Computer Aided Design (CAD) solid model. Then, the CFD solver FLUENT was used to solve the governing equations of fluid dynamics and heat transfer to obtain the solutions that can provide temperature distributions (steady calculations) and performance cycle analysis (transient calculations). Numerous other commercial solver tools were researched before FLUENT was chosen to analyze this problem.[5,6]

During the solution of this model, the ASC–E2 computational model was divided into as many as 20 parts, and calculations were performed in parallel on a multiprocessor computer shown in Fig. 6.. During a prior parametric study of parallel computing efficiency, it was determined that for large simulations, calculations can be performed more efficiently if the problem is divided in a manner such that each processor has between 300,000 to 450,000 grid points.

Figure 6. NASA GRC Opteron Cluster with Myrinet Optical Communications.

IV. Parallel Computing

The complexity of the ASC–E2 computational model places high demands on computer resources. The largest model presented here, consisted of 8 million grid points and required somewhere between 15 to 20 processors for a timely solution. The NASA Opteron computer cluster was delivered to NASA from DOE and was manufactured by Atipa and Microway. It serves as a computational testbed for fluid-structure analysis of Stirling convertors and its components, and became fully functional at GRC in 2007. The cluster consists of 374 processors on a 160-channel Clos network. The fiber optics provided a speed of 1.28 Gb/s bi-directional with a 600 ns latency. The cluster has a total memory of 40 TeraBytes and utilizes 75 kVA of power and 20 tons of cooling.

Previous parametric studies on the computational efficiency of the cluster revealed that no more than 25 to 30 processors should be used for a single simulation. However, it is possible to calculate several multiple-processor cases simultaneously.

V. Convertor Operating Assumptions

Linear Alternator Losses

During the operation of this convertor, the mechanical power generated by the piston is converted into electrical power by the linear alternator that is driven by the piston. Conversion of mechanical power to electrical power is not 100% efficient. The difference between the mechanical power created by the piston and the electrical power converted by the linear alternator is referred to as linear alternator losses. These losses are distributed throughout the convertor in the forms of eddy, hysteresis, and coil losses. The estimated distribution of the linear alternator losses are shown in Fig. 7.

The mechanical power generated by the Stirling cycle was estimated by

$$W_{mech} = W_e/\eta_{LA} \tag{1}$$

where the linear alternator conversion efficiency (η_{LA}) was assumed to be a constant in every case. Then, the power loss during power conversion of the linear alternator from mechanical to electrical power can be obtained by the difference

$$W_{LOSS} = W_{mech} - W_e \tag{2}$$

For these analyses, it was assumed that the linear alternator losses could be simulated by applying it as a heat generation rate inside the coil of the linear alternator. This heat generation rate in the coil was applied as a boundary condition in all of the computational simulations.

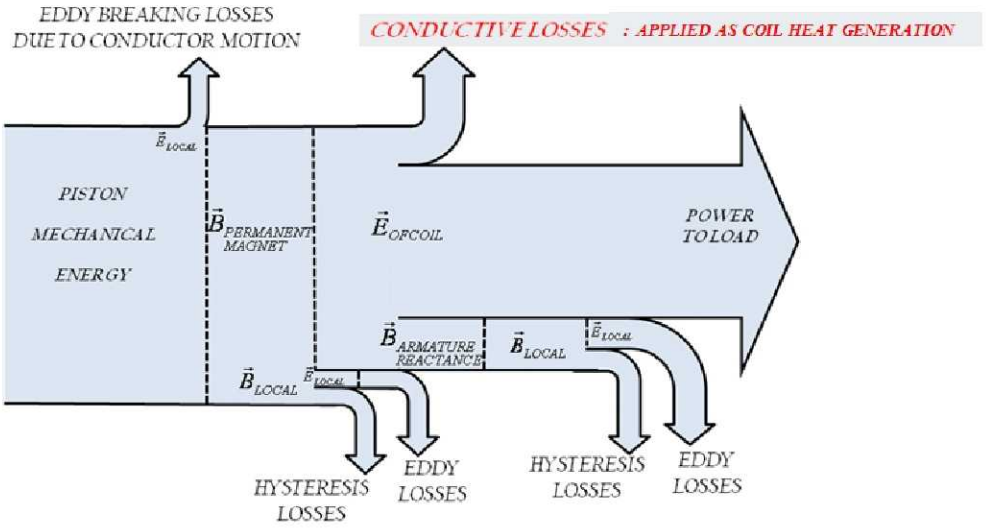

Figure 7. Loss distribution during mechanical-to-electrical power conversion.

Regenerator Modeling

Another important and complicated component in this convertor is the porous regenerator. By the way that it is constructed, a regenerator can have roughly 3 to 40 times more effective heat transfer than a typical solid material. The inaccurate modeling of this particular component can affect the calculated performance of the entire Stirling cycle. Dyson et al. utilized a Representative Elementary Volume (REV) and some closure equations[5,7] that were partially derived from experiments and microscale (pore level) numerical simulations to obtain a source term equation that can be added to the momentum equations. This source term only enforces the pressure drop through the regenerator in accordance to the Darcy-Forcheimer equation. A single source term, shown in Eq. 3, is applied to each of the momentum equations (for $i = x, y, or z$), where

$$S_i = -\left(\frac{\mu}{K} v_i + C_2 \frac{1}{2} \rho v_{mag} v_i\right) \tag{3}$$

Permeability K and C_2, as well as the inertial coefficient C_f were determined experimentally. In the energy equation, the standard energy transport equation is solved for porous media regions with modifications to the conduction flux and the transient terms only. The conduction flux uses an effective conductivity and the transient term includes the thermal inertia of the solid region on the medium. The effective thermal conductivity is defined in the commercial code FLUENT as

$$k_{eff} = \gamma k_{fluid} + (1 - \gamma) k_{solid} \tag{4}$$

In this case, the isotropic contributions from the fluid are added to the diagonal elements of the solid anisotropic thermal conductivity matrix.

VI. Boundary Conditions

There are three different series of boundary conditions that were applied to the ASC–E2 computational model. They include

1) Laboratory Conditions—These conditions are an effort to compare the preliminary simulation results with test observations from the NASA GRC's Stirling Research Laboratory.
2) Sterilization Conditions (Preflight)—These conditions include preflight conditions that may be performed on the convertor to remove contaminants that could have an adverse effect on the target mission environment.
3) Mission Conditions—These conditions represent four different stages of operation, which includes two at the beginning of mission (BOM) and two at the end of mission (EOM).

These computational models (both axi-symmetric and three dimensional) have the capability of generating transient solutions to simulate cyclic operation, as they are both equipped with sliding mesh interfaces and deforming meshes. The static solutions shown here are a natural precursor to the transient calculations that will be performed in the future.

Boundary Condition Set Number 1—Laboratory Conditions

Tests were in progress for the ASC–E at this set of conditions. As mentioned before, the ASC-E is an earlier version of the convertor that was tested at numerous conditions. At a snapshot in time, the convertor had a hot-end temperature of 624 °C and a cold-end temperature of 63.2 °C. A total of two ASC–E convertors were inside of the ASRG while this research was being conducted. The convertors were surrounded with an argon environment while inside of the ASRGs, and the ASRGs were subject to laboratory temperatures (~20 °C). At this time, a convertor was producing 62.72 W_e and the external wall temperature of the pressure vessel was measured at 67.8 °C (Table 1).

Table 1. ASC–E convertor measured data.

MODEL CONFIGURATION	AVAILABLE DATA	ENVIRONMENT		BOUNDARY CONDITIONS		MEASURED VALUE
MODEL	TYPE	SURROUNDING MEDIUM	ENVIRONMENT TEMPERATURE	THOT °C	TCOLD °C	PV °C
ASC-E	Experimental Results	ARGON	20	624	63.2	**67.8**

Although the computational model that was used was for the ASC–E2, there are numerous common internal components. So while an exact match was not expected, it was assumed that the computational temperature results would be in the same vicinity as those observed during the experiments.

Boundary Condition Set Number 2—Sterilization Conditions

The purpose of using this series of conditions was to make sure that internal temperature (of the magnet) did not exceed its limits. There is a danger of demagnetization if the temperature exceeds a limit that was understood to be up to 150 °C. Using this series of conditions, the goal is to see how the model predicts magnet temperatures when in an argon environment and subject to a 110 °C sterilization temperature. This is more aggressive than the anticipated normal operating environment of the convertor, but is a necessary preflight step in eliminating contamination during the mission. Nominal conditions are used (hot-end and cold-end temperatures of 850/90 °C) during model simulations.

Boundary Condition Set Number 3—Expected Mission Conditions

At the time these computational simulations were performed, boundary conditions from the January-7-2010 ASC–E2 Product Specification were available, and are shown in Table 2. There were two conditions representing the BOM and two conditions representing the EOM.

Table 2. ASC–E2 Product Specification data. (version from January 7, 2010)

Mission Stage	Condition	Qin *Watts*	T_{HOT} *°C*	T_{COLD} *°C*	T_{PV} *°C*	W_e *Watts*
BOM	1	208	≤ 850	52	61	84.5
BOM	2	208	≤ 850	90	98	79.5
EOM	1	182	≤ 850	36	44	75.3
EOM	2	182	≤ 850	90	98	69.2

In previous simulations, the target temperatures were applied in the appropriate locations. However, for this series of boundary conditions (Set Number 3), heat input into the heat collector was one of the boundary conditions (instead of the 850 °C acceptor outer plane temperature) at the hot end. The cold temperature was applied at the CSAF—outer rejector interface in the same manner as all of the other simulations.

For the simulations model, the generalized internal components of the ASC are shown in Fig. 8, and the key measurement locations are shown in Fig. 9. However, the exact geometry of the components used in these analyses are not illustrated..

VII. Results From Statically Simulated Convertor

For this type of problem, a steady solution needs to be generated first to calculate the approximate temperature profile. While the relevant internal components are not in motion, all of the relevant thermal loads are in place which includes

- Hot end: Heater head temperature or heat flux added (Q_{IN})
- Cold end: CSAF temperature or heat flux removed
- Coil heat generation: Linear alternator losses

With these boundary conditions applied, attention was paid to the external wall of the pressure vessel (which is part of the experimental measurements) and the magnet temperatures (which are not part of the experimental measurements).

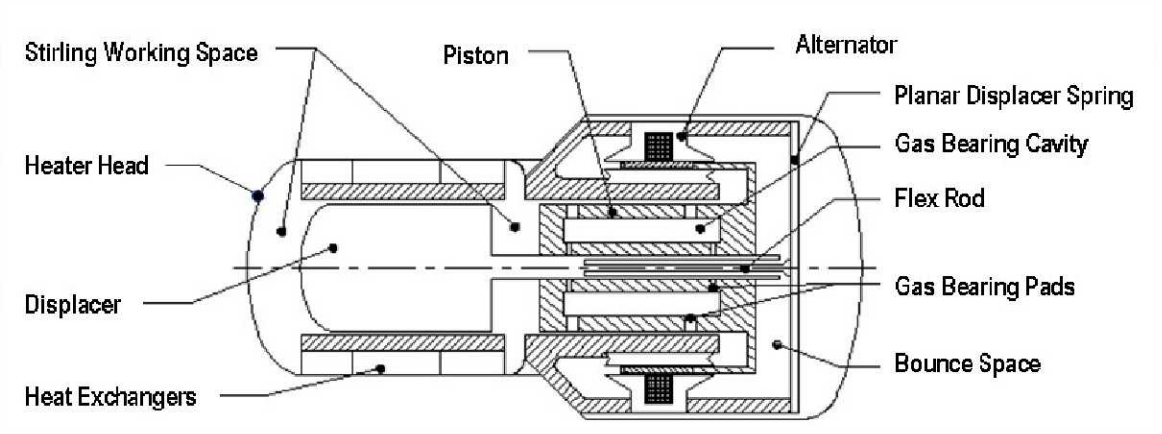

Figure 8. ASC convertor components.

Boundary Condition Set Number 1—Laboratory Conditions

The calculated results of the ASC–E2 axisymmetric model are included in Table 3. They are compared to the experimental results of the ASC–E, which has numerous overlapping internal components. At the time this model was developed, the ASC–E2 was still being constructed and was not available for experimental testing yet. Any computational results that are produced at this time had to be compared to experimental results of a previous ASC-E model until the ASC–E2 became available for testing.

The development of the ASC–E2 computational model went through various stages. The first stage included constructing an axisymmetric model. This axisymmetric model was used along with the testing conditions of the ASC–E to obtain the first set of results for Boundary Condition Set Number 1. The model was surrounded by an argon environment with a remote boundary that was used to apply a temperature boundary condition. For this test, the remote boundary condition was set for 20 °C.

After these conditions were applied to the computational model, the computational model was run until steady-state conditions were achieved, resulting in the calculated external temperature on the pressure vessel wall of 69.1 °C (compared to the 67.8 °C measured on the ASC–E). There are many aspects that could explain this difference, which would include the coil heat generation boundary condition, or that the thermocouples have an accuracy of ±2 °C. The heat generation term was based on the unconverted energy of the 80 W_e ASC–E2, which may be greater that the unconverted energy of the 62.72 W_e of the ASC–E. The result is a higher pressure vessel exterior wall temperature than that observed from experimental results.

Boundary Condition Set Number 2—Sterilization Conditions

This condition was analyzed to look at the sterilization procedure that the convertor may be subjected to. There is no experimental data at this time to compare to the computational results. The ASC will be

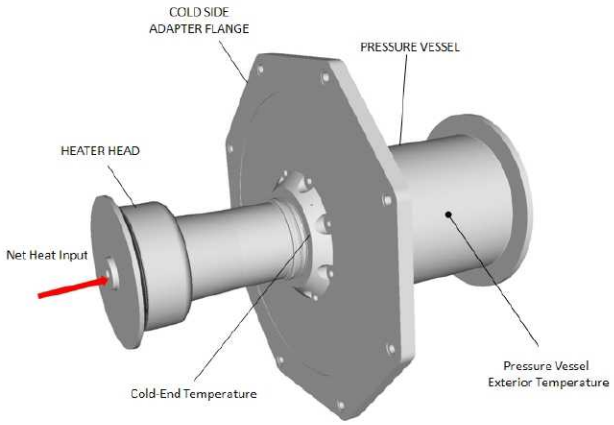

Figure 9. ASC–E2 and some indicated positions of interest.

Table 3. Pressure vessel wall temperature comparison between experimental and calculated results

MODEL CONFIGURATION	AVAILABLE DATA	ENVIRONMENT		BOUNDARY CONDITIONS		MEASURED VALUE	CALCULATED VALUE
MODEL	TYPE	SURROUNDING MEDIUM	ENVIRONMENT TEMPERATURE	THOT °C	TCOLD °C	PV °C	PV °C
ASC-E	Exp and Comp	ARGON	20	624	63.2	**67.8**	69.1

placed in a 110 °C environment of argon for a predetermined period of time. For this simulation, the remote boundary of the computational space was set to 110 °C, while the hot end was set to 850 °C. Because the required heat removal rate that would produce a cold-end temperature of 120 °C was not known, a parametric series of solutions were generated. The nominal power produced by the convertor was assumed to be 80 W_e.

Table 4. ASC–E2 axisymmetric model results (varying coil heat generation)

MODEL CONFIGURATION			ENVIRONMENT	APPLIED BOUNDARY CONDITIONS		COIL HEAT GENERATION	PV External Wall
MODEL	TYPE	BEHAVIOR	TEMPERATURE	THOT °C	TCOLD °C	Watts	°C
ASC-E2	AXI	Stationary	110	850	120	7	*132.7*
	AXI	Stationary	110	850	120	8	*134.0*
	AXI	Stationary	110	850	120	**10**	***137.0***
	AXI	Stationary	110	850	120	11	*138.6*
ASC-E2	3D	Stationary	110	850	120	**10**	***135.7***

Table 5. ASC–E2 model results (varying cold end temperature)

MODEL CONFIGURATION			ENVIRONMENT	APPLIED BOUNDARY CONDITIONS		COIL HEAT GENERATION	PV External Wall
MODEL	TYPE	BEHAVIOR	TEMPERATURE	THOT °C	TCOLD °C	Watts	°C
ASC-E2	AXI	Stationary	110	850	120	10	*137.0*
	3D	Stationary	110	850	120	10	*135.7*
	AXI	Stationary	110	850	130	10	*142.5*
	AXI	Stationary	110	850	140	10	*147.0*
ASC-E2	AXI	Stationary	110	850	120	11	*139.6*
	AXI	Stationary	110	850	130	11	*144.2*
	AXI	Stationary	110	850	140	11	*148.8*

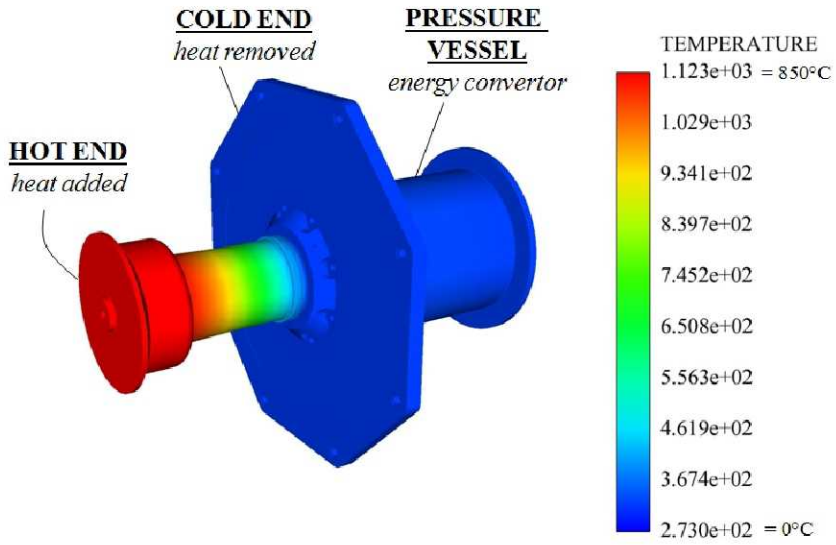

Figure 10. ASC–E2 three-dimensional model: calculated temperature contours.

The cold-end temperatures were set to values of 120 °C and the heat generated by the coil was varied from 7 to 11 W. The mid-span pressure vessel exterior wall temperature varied from 132.7 to 138.6 °C. Calculations were also performed on the three-dimensional model with 10 W of heat generation applied to the coil as a boundary condition.

The pressure vessel exterior wall temperatures for the three-dimensional calculations were 1.3 °C lower than that predicted by the axisymmetric model. The results of these calculations are shown in Table 4.

Another series of calculations was performed with the axisymmetric model. For this series of calculations, the coil heat generation boundary condition was held constant while the cold-end temperature was varied from 120 to 140 °C. This was done with the coil generating 10 and 11 W of heat. The results of this series of calculations are shown in Table 5.

For the lowest heat generation rates shown in Table 4 (7 and 8 W), the external wall of the pressure vessel was 13 and 14 °C higher than the cold-end temperature. The temperature on the external pressure vessel wall tended to be within 1-2 °C of the peak magnet temperature in these simulations. If it is assumed that the heat rejection at the cold end is such that the cold-end temperature is maintained at 110 °C, then the peak magnet temperature would most likely not exceed 15 °C above the cold-end temperature (for T_{cold} = 110 °C).

Boundary Condition Set Number 3—Expected Mission Conditions

These conditions represent a possible set of conditions that the convertor will be subjected to during its mission. For these simulations, a radiating pressure vessel exterior wall boundary condition was applied with a remote temperature that is 25 °C less than the cold-end temperature for each case. The expected power outputs are 84.5 W_e (BOM–1), 79.5 W_e (BOM–2), 75.3 W_e (EOM–1), and 69.2 W_e (EOM–2). The expected power output and the linear alternator efficiency were used to estimate a different coil heat generation boundary condition, and will not be discussed here. Table 6 shows the calculated results of these conditions when

Table 6. ASC–E2 calculated results of Product Specification data (using the three-dimensional model)

MISSION PHASE	CONDITION	FAR-FIELD TEMPERATURE	DESIGN INTENT VALUES			MODEL VALUES	
			THOT °C	TCOLD °C	PV °C	PV-AXI °C	PV-3D °C
BOM	1	27	850	52	**61**	**65.8**	**62.5**
BOM	2	65	850	90	**98**	**97.5**	**97.9**
EOM	1	11	850	36	**44**	**55**	**45.7**
EOM	2	65	850	90	**98**	**95.9**	**96.2**

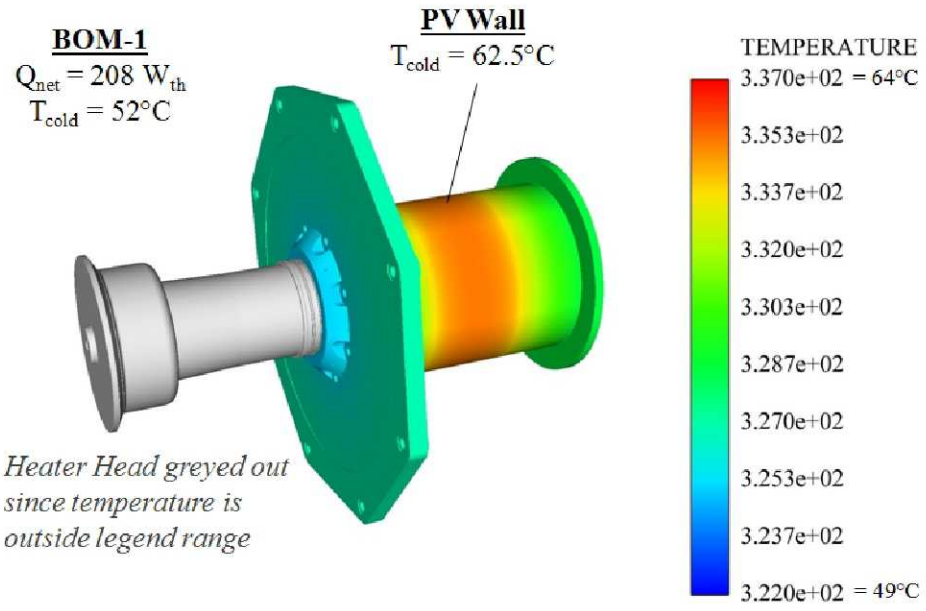

Figure 11. ASC–E2 three-dimensional model: calculated temperature contours from BOM–1.

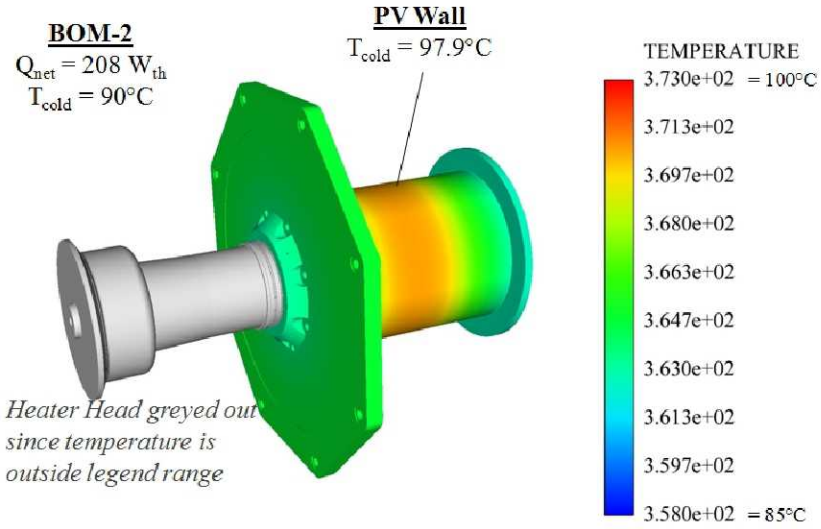

Figure 12. ASC–E2 three-dimensional model: calculated temperature contours from BOM–2.

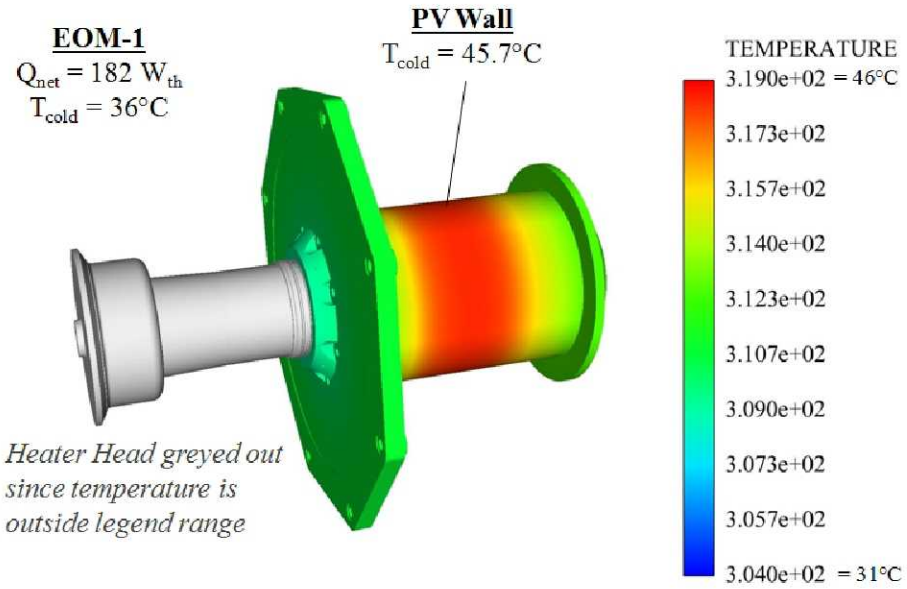

Figure 13. ASC–E2 three-dimensional model: calculated temperature contours from EOM–1.

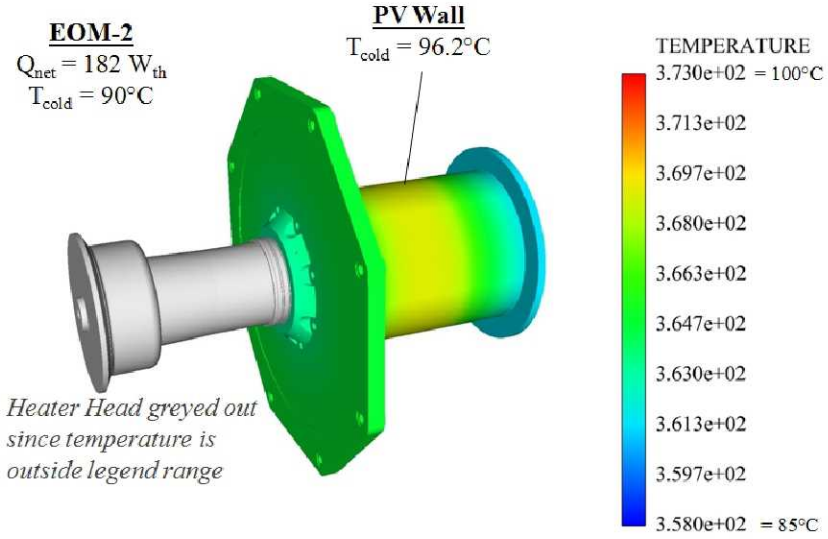

Figure 14. ASC–E2 three-dimensional model: calculated temperature contours from EOM–2.

Table 7. ASC–E2 calculated results of product specification data (using the three-dimensional model)

MISSION PHASE	CONDITION	FAR-FIELD TEMPERATURE	DESIGN INTENT VALUES			MODEL VALUES		
			THOT °C	TCOLD °C	PV °C	COIL °C	MAGNET °C	PV °C
BOM	1	27	850	52	61	64.4	63.0	62.5
BOM	2	65	850	90	98	99.9	98.7	97.9
EOM	1	11	850	36	44	47.3	46.0	45.7
EOM	2	65	850	90	98	98.0	97.0	96.2

using both the axisymmetric and the three-dimensional computational model. Both models produced temperatures that were close to the design intent values, although the three-dimensional model produced temperatures that were closer to the expected peak pressure vessel exterior surface temperatures.

Table 7 shows a summary of the cases run and includes the calculated peak coil, peak magnet, and peak pressure vessel exterior wall temperatures. Exterior views of the temperature contours of each case can be seen in Figs. 11 to 14.

VIII. Summary

A solid CAD model of the ASC, which is a major component in the ASRG, was used to create fully functional stationary (not operating) and moving (operating) axisymmetric and three-dimensional computational models, that were compared to experimental data produced by an earlier version of the convertor (ASC–E). Then, the numerical models were used to investigate two conditions that the convertor is likely to experience during a space mission.

Simulation With ASC–E Conditions

The ASC–E was considered to be a good test since there are numerous similarities (relative to the dimensions and material composition) to the ASC–E2. The computational model of the ASC–E2 (applying the experimentally observed temperatures from the ASC–E tests as a boundary condition) resulted in a pressure vessel exterior wall temperature that was only 1.3 °C higher than the experimentally observed results.

Simulations at Sterilization Conditions

The numerical simulation was run at applied conditions that represent the sterilization phase, which the convertor may be subjected to remove contaminants prior to space missions to deep space environments. For a sterilization procedure in a 110 °C argon environment (with a cold-end temperature of 110 °C), calculation trends showed that the peak magnet temperature would not exceed 15 °C above the cold-end temperature of 110 °C, which would ensure that the magnets remain at a safe condition.

When the cold-end temperature was set at 120 °C and the ideal (nominal) linear alternator efficiency was applied, the peak pressure vessel surface temperature was 12.7 °C above the cold-end temperature. Increases in coil heat generation rate resulted in an increase in the external pressure vessel wall temperature at a rate of 1.4 °C per W.

Fixing the coil heat generation rate at 10 W and increasing the cold-end temperature resulted in an exterior pressure vessel wall temperature increase at a rate of 5 per 10 °C increase in cold-end temperature.

Anticipated ASC Mission Performance Conditions

Application of the ASC–E2 performance data from the ASC–E2 Product Specification document (version dated Jan. 7, 2010), four conditions were run with the three-dimensional model. The peak temperature variation of the exterior wall of the pressure vessel for the four different boundary conditions (BOM–1, BOM–2, EOM–1, and EOM–2) ranged from ±1.8 °C relative to the anticipated values from the Product Specification document.

The fidelity of these computational models will continue to be enhanced so that future advanced computational simulations can continue to add to the understanding of details of the operating conditions that cannot be measured experimentally, or might put high-value hardware at risk. Furthermore, in some cases, these models can be used to explore results of operating scenarios or design changes more quickly than tests that require hardware modifications.

References

1. Shaltens, R. K., "Future Opportunities for Dynamic Power Systems for NASA Missions," 2007, NASA TM–214707.
2. Schreiber, J. G., "Status of the NASA Stirling Radioisotope Project," 2007, NASA TM–214804.
3. Shaltens, R. K. and Wong, W. A., "Advanced Stirling Technology Development at NASA Glenn Research Center," 2007, NASA TM–214930.
4. Oleson, S., et al., "Radioisotope Electric Propulsion Centaur Orbiter Spacecraft Design Overview," 2009, NASA TM–215488.
5. Dyson, R. W., Wilson, S. D., Tew, R. C., and Demko, R., "Fast Whole-Engine Stirling Analysis," 2005, NASA TM–213960.
6. Dyson, R. W., Wilson, S. D., Tew, R. C., and Demko, R., "Stirling Analysis Comparison of Commercial Versus High-Order Methods," 2005, NASA TM–213976.
7. Tew, R. C., Dyson, R. W., Wilson, S. D., and Demko, R., "Overview 2004 of NASA-Stirling Convertor CFD Model Development and Regenerator R&D Efforts," 2004, NASA TM–213404.